Atmos. Chem. Phys. Discuss., doi:10.5194/acp-2015-1058, 2016
Manuscript under review for journal Atmos. Chem. Phys.
Published: 17 February 2016

Atmospheric Chemistry and Physics Discussions

Differential Column Measurements Using Compact Solar-Tracking Spectrometers

Jia Chen[1,4], Camille Viatte[2], Jacob K. Hedelius[2], Taylor Jones[1], Jonathan E. Franklin[1], Harrison Parker[3], Elaine W. Gottlieb[1], Paul O. Wennberg[2], Manvendra K. Dubey[3], and Steven C. Wofsy[1]

[1]School of Engineering and Applied Sciences and Department of Earth and Planetary Sciences, Harvard University, Cambridge, MA 02138, USA
[2]Division of Geological and Planetary Sciences, California Institute of Technology, Pasadena, CA 91125, USA
[3]Earth and Environmental Sciences, Los Alamos National Laboratory, Los Alamos, NM 87545, USA
[4]now at Electrical and Computer Engineering, Technische Universität München, Munich, 80333, Germany

Correspondence to: Jia Chen (jia.chen@tum.de)

Abstract. We demonstrate the use of compact solar-tracking Fourier transform spectrometers (Bruker EM27/SUN) for differential measurements of the column-averaged dry-air mole fractions of CH_4 and CO_2 within urban areas. Using Allan variance analysis, we show that the differential column measurement has a precision of 0.1‰ for X_{CO_2} and X_{CH_4} using an optimum integration time of 10 min, which corresponds to standard deviations of 0.04 ppm, and 0.2 ppb, respectively. The sensor system is very stable over time and after relocation across the continent. We report tests of the differential column measurement, and its sensitivity to emission sources, by measuring the downwind minus upwind column gradient ΔX_{CH_4} across dairy farms in the Chino California area and using the data to verify emissions reported in the literature. Spatial column gradient ratios $\Delta X_{CH_4}/\Delta X_{CO_2}$ were observed across Pasadena within the Los Angeles basin, indicating values consistent with regional emission ratios from the literature. Our precise, rapid measurements allow us to determine significant short-term variations (5-10 minutes) of X_{CO_2} and X_{CH_4}, and to show that they represent atmospheric phenomena.

Overall, this study helps establish a range of new applications for compact solar-viewing Fourier transform spectrometers. By accurately measuring the small differences in integrated column amounts across local and regional sources, we directly observe the mass loading of the atmosphere due to the influence of emissions in the intervening locale. The inference of the source strength is much more direct than inversion modeling using only surface concentrations, and less subject to errors associated with small-scale transport phenomena.

1 Introduction

Cities and their surrounding urban regions are home to 54% of the world population (WHO (2014)) and account for $\sim$ 70% (UNHabitat (2011)) of total fossil fuel emissions. Hence, accurate methods for measuring urban and regional scale carbon fluxes are required in order to design and implement policies for emissions reduction initiatives.

It is challenging to use *in situ* measurements of CO_2 and CH_4 to derive emission fluxes in urban regions. Surface concentrations typically have high variance due to the influence of nearby sources, and they are strongly modulated by mesoscale

Atmos. Chem. Phys. Discuss., doi:10.5194/acp-2015-1058, 2016
Manuscript under review for journal Atmos. Chem. Phys.
Published: 17 February 2016

Atmospheric Chemistry and Physics Discussions

transport phenomena that are difficult to simulate in atmospheric models. These include the variation of the depth of the planetary boundary layer (PBL), sea breeze, and topographic flows, etc. (McKain et al. (2012); Bréon et al. (2015)).

The mass loading of the atmosphere can be directly determined by measuring the column integrated amount of a tracer through the whole atmosphere. Column measurements are insensitive to vertical redistribution of tracer mass, e.g. due to growth of the PBL, and are also less influenced by nearby point sources whose emissions are concentrated in a thin layer near the surface. Column observations are more compatible with the scale of atmospheric models and hence provide stronger constraints for inverse modeling (Lindenmaier et al. (2014)).

One potential drawback, however, is that column observations are sensitive to surface emissions over a very wide range of spatial scales, spanning nearby emissions and all those upwind in the urban, continental, and hemispheric domains. In this paper we demonstrate how to use simultaneous measurements of the column-averaged dry-air mole fractions (DMFs) of CH_4 and CO_2 (denoted by X_{CH_4} and X_{CO_2}, respectively) at upwind and downwind sites to mitigate this limitation. The horizontal gradients *within* a region are relatively insensitive to surface fluxes upwind of the domain, providing favorable input for regional flux inversions.

We use three matched, compact Fourier Transform spectrometers to measure the small (1‰) differences of X_{CH_4} and X_{CO_2}, and we demonstrate sufficient precision and speed to determine emission rates at the urban scale. By directly measuring spatial and temporal gradients of the mass loading, we reduce the sensitivity of inverse model results to atmospheric fine structure, such as may arise from vertical redistribution of trace gases, and that often complicates interpretation of surface *in situ* data (Chang et al. (2014)).

Our ground-based network of spectrometers measuring gradients of column amounts could enable new approaches to validate the *urban-rural gradients* of satellite observations such as OCO-2 (Crisp et al. (2008); Frankenberg et al. (2015)) and TROPOMI (Veefkind et al. (2012)). In contrast to the large, high spectral resolution instruments of the Total Carbon Column Observing Network (TCCON), which are not easily re-located, the compact spectrometers can be deployed directly under satellite tracks that pass near major cities, to assess potential artifacts in satellite-derived tracer gradients that might arise from urban or rural differences in aerosol burden, land surface properties, etc.

Several recent papers have studied column-averaged concentrations of trace gases to derive source fluxes. Wunch et al. (2009) observed diurnal patterns for X_{CO_2}, X_{CH_4}, and X_{CO} over Los Angeles, similar to the model simulations of McKain et al. (2012) for Salt Lake City. Kort et al. (2012) used GoSAT satellite data to measure the difference between CO_2 columns inside and outside Los Angeles, and to derive a top-down inventory for CO_2. Papers by Stremme et al. (2009, 2013) and Té et al. (2012) used total column measurements from a ground-based Fourier transform spectrometer (FTS) to estimate and monitor CO emission in Mexico City and Paris, respectively. Mellqvist et al. (2010) studied plumes from industrial complexes, and Lindenmaier et al. (2014) examined plumes from two power plants and discriminated them. Kort et al. (2014) quantified large methane sources missing in inventories at Four Corners, NM. However, these studies did not have simultaneous upwind and downwind column data, one of the novel elements of the present paper.

Frey et al. (2015) and Hase et al. (2015) reported deployments of multiple FTSs of the same type as employed here, deriving calibration and stability characteristics in a field setting. We extend this analysis by determining the Allan variances of column

Atmos. Chem. Phys. Discuss., doi:10.5194/acp-2015-1058, 2016
Manuscript under review for journal Atmos. Chem. Phys.
Published: 17 February 2016

Atmospheric Chemistry and Physics Discussions

concentration *differences* between spectrometer pairs deployed side-by-side, providing a rigorous assessment of the precision of the differential column measurements.

Here we study local scale gradients in X_{CO_2} and X_{CH_4} in two applications. First, we deployed our spectrometers upwind and downwind of the dairy farms in Chino, California (about 50 km^2 area), and use the data to compare with emissions reported in the literature. A second application uses the observed ratio of differences in X_{CO_2} and X_{CH_4}, i.e. $\Delta X_{CH_4}/\Delta X_{CO_2}$, to characterize emission ratios for these gases within the Los Angeles basin.

In another application of the compact spectrometers, we co-located spectrometers to demonstrate measurement of short-term (5-10 minutes) variations of column-averaged DMFs in the atmosphere. The high precision measurements with rapid scan rates are an advantage of the compact spectrometers compared to larger, higher spectral resolution spectrometers. We show that high frequency observations can be used to quantify the influence of sporadic events, such as plumes within the PBL or instabilities across the top of the mixed layer (ML), on measurements in urban areas.

2 Differential Column Network

Our differential column network uses at least two spectrometers to make simultaneous measurements of column number densities of CO_2, CH_4, and O_2. We then compute the column-averaged DMFs (Wunch et al. (2011)) and gradients for a gas G, i.e., $\Delta X_G = X_G^d - X_G^u$, where X_G^d and X_G^u stand for column-averaged DMFs at downwind and upwind sites.

Our sensors are two EM27/SUN FTS units owned by Harvard University, and one owned by Los Alamos National Laboratory, #45, 46, and 34 Bruker Optics (designated *ha*, *hb*, and *pl*, respectively). They are compact (62.5 cm $\times$ 35.6 cm $\times$ 47.3 cm) and light-weight (22.8 kg including the sun tracker), with spectral resolution of 0.5 cm^{-1} and a forward/backward scan time of 5.8 s. The EM27/SUN tracks the sun precisely (1 σ: 11 arc s) using a camera for fine alignment of the tracking mirrors (Gisi et al. (2011)). It is mechanically very robust, with excellent precision in retrieving X_{CO_2} and X_{CH_4} (Gisi et al. (2012)), comparable to Bruker 125HR used in the TCCON network (Wunch et al. (2011)).

We carried out extensive side-by-side measurements of *ha* and *hb* in Boston and Pasadena, over many months, thoroughly examining precision and robustness, and also compared these systems to the TCCON spectrometer in Pasadena, California (Hedelius et al. (2016)). We confirm that these spectrometers are extraordinarily stable (Frey et al. (2015)). We show that comparing pairs of them cancels out most of the systematic error and bias from diverse sources, e.g. spectroscopic and retrieval errors, instrument bias, and errors in pressure and temperature, enabling us to determine 1‰ differences in column-averaged DMFs across the network.

Atmos. Chem. Phys. Discuss., doi:10.5194/acp-2015-1058, 2016
Manuscript under review for journal Atmos. Chem. Phys.
Published: 17 February 2016

Atmospheric Chemistry and Physics Discussions

3 System Characterization

3.1 Assessing System Precision

Known standards cannot be exchanged for the ambient air in a total column measurement, hence it is difficult to assess the precision of atmospheric measurements end-to-end. Two commonly used literature methods for precision estimates have been based on:

1. *Measurements of the standard deviation of the DMF time series, with the trend removed subtracting a moving average (Gisi et al. (2012)).* This approach is confounded by real variations in the atmosphere that occur on short time scales (*vide infra*).

2. *The residual of the spectral fit.* This estimate does not separate systematic errors, e.g. errors in spectroscopic database and modeling of instrument line shape, from the measurement noise, and therefore may underestimate the true precision (*cf.* Fu et al. (2014)).

In this paper we use the Allan variance method (Allan (1966), Werle et al. (1993)) to estimate the measurement precision. Fig. 1 shows the Allan standard deviations of the *differences* in column-averaged DMFs measured simultaneously by *ha* and *hb* at the same location, i.e, $\Delta X_G(t) = X_G^{hb}(t) - X_G^{ha}(t)$. The Allan variance of ΔX_G is denoted by $\sigma^2_{allan,\Delta X_G}$, which is the expectation value $\langle\rangle$ of the difference between adjacent samples averaged over the time period τ:

$$\sigma^2_{allan,\Delta X_G}(\tau) = \frac{1}{2}\left\langle(\overline{\Delta X_{G,n+1}} - \overline{\Delta X_{G,n}})^2\right\rangle, \quad (1)$$

with $\overline{\Delta X_{G,n}} = \frac{1}{\tau}\int_{t_n}^{t_n+\tau} \Delta X_G(t)dt$. Practically $\overline{\Delta X_{G,n}}$ is the mean of all ΔX_G measurements within the time interval $[t_n, t_n+\tau)$.

According to the Allan variance plots:

- The optimal integration time, given by the minimum in the Allan standard deviation, is 10 to 20 min, for both X_{CO_2} and X_{CH_4}.

- When averaging 10 min, the precision (1 standard deviation) of the EM27/SUN differential column measurement is 0.04-0.05 ppm (0.1‰) for X_{CO_2} and 0.1-0.2 ppb (0.1‰) for X_{CH_4}. Since the two instruments are statistically uncorrelated, the individual measurement noise is smaller by factor $1/\sqrt{2}$, indicating precision comparable to near infrared *in situ* laser spectrometers with commensurate optical path length and integration time (Picarro (2015a, b)). Note that these precision estimates represent the full end-to-end processing of the observations, including deriving the spectrum from the interferogram, retrieving the column number densities in the atmosphere, and normalizing with the O_2 column amount to obtain the column-averaged DMFs.

- When integrating less than 10 min, the Allan standard deviation follows a slope of -1/2 in the double logarithmic scale, indicating white noise ($\tau^{-1/2} \rightarrow f^0$), which has a constant power spectral density over the frequency f. As the averaging time τ increases beyond 10 min, the Allan standard deviation rises a little, showing a small color noise component

Atmos. Chem. Phys. Discuss., doi:10.5194/acp-2015-1058, 2016
Manuscript under review for journal Atmos. Chem. Phys.
Published: 17 February 2016

Atmospheric Chemistry and Physics Discussions

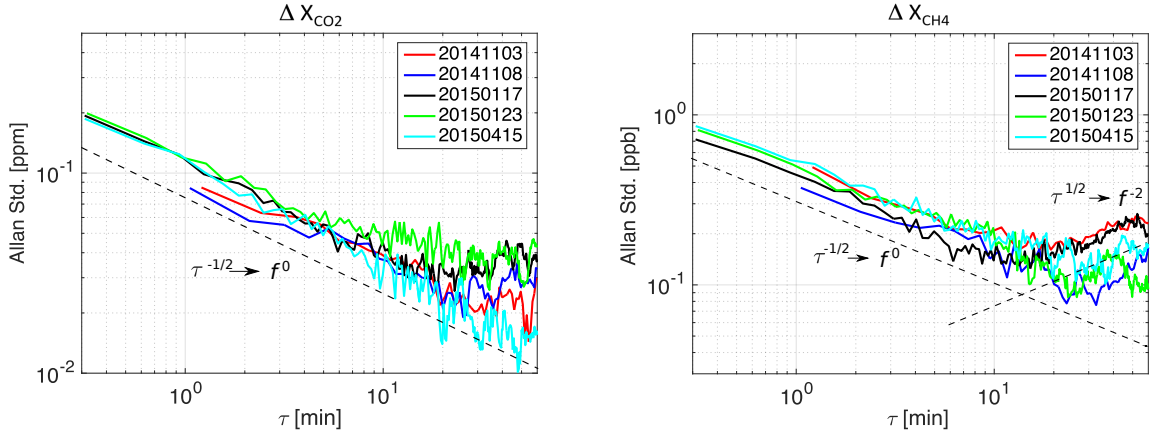

Figure 1. Allan standard deviation $\sigma_{allan,\Delta X_{CO2}}$ and $\sigma_{allan,\Delta X_{CH4}}$ as a function of the integrating time τ. The black dashed lines represent a slope of $-1/2$ and a slope of $1/2$, which correspond to power spectral densities $S(f) = f^0$ (white noise) and $S(f) = f^{-2}$ (Brownian noise), respectively. The Allan standard deviation follows a slope of $-1/2$ up to an integration time of 10 to 20 min, and then stays constant ($S(f) = f^{-1}$), and subsequently turns over to a slope of $1/2$, which describes a linear drift.

($\tau^{1/2} \rightarrow f^{-2}$), which arises from instrument drift, in part due to temperature differences inside of the spectrometers. There is also a small divergence between the measurements of ha and hb at high solar zenith angles, traceable to their slightly different instrument line shapes (ILSs). The measured ILS parameters are given in Appendix A. Microscale eddies have durations of 10 s to 10 min and length scales from tens to hundreds of meters (Stull (1988), Fig. 2.2). Therefore atmospheric turbulence probably does not play a major role in the Allan plot because there is little color noise within time scale $\leq$ 10 min for two spectrometers looking along atmospheric paths separated by only a few meters.

We use a shorter integration time (5 min) for measuring emissions from local and regional scale sources (Sec. 4.1 and 4.2), in order to retain high frequency atmospheric signals, giving us precision of 0.05-0.06 ppm for ΔX_{CO_2} and 0.2-0.3 ppb for ΔX_{CH_4} (see Fig. 1). To study the short-term variations due to pollution plumes or turbulent eddies we use 2 min integration time (Sec. 4.3).

3.2 System Robustness

Column gradient observations by two spectrometers will inevitably have bias in addition to fluctuations and drift. For the EM27/SUN, small differences in the alignments of the interferometers result in minute, but observable and systematic, deviations in the retrieval results. We examined the biases between ha and hb over a long period of time to determine if these errors can be effectively corrected by applying a constant scaling factor to the retrieval of one instrument to match the performance of the other. The scaling factors are determined assuming a linear model, i.e. $X_G^{hb} = X_G^{ha} \cdot \overline{R_G}$, and for each gas individually.

Atmos. Chem. Phys. Discuss., doi:10.5194/acp-2015-1058, 2016
Manuscript under review for journal Atmos. Chem. Phys.
Published: 17 February 2016

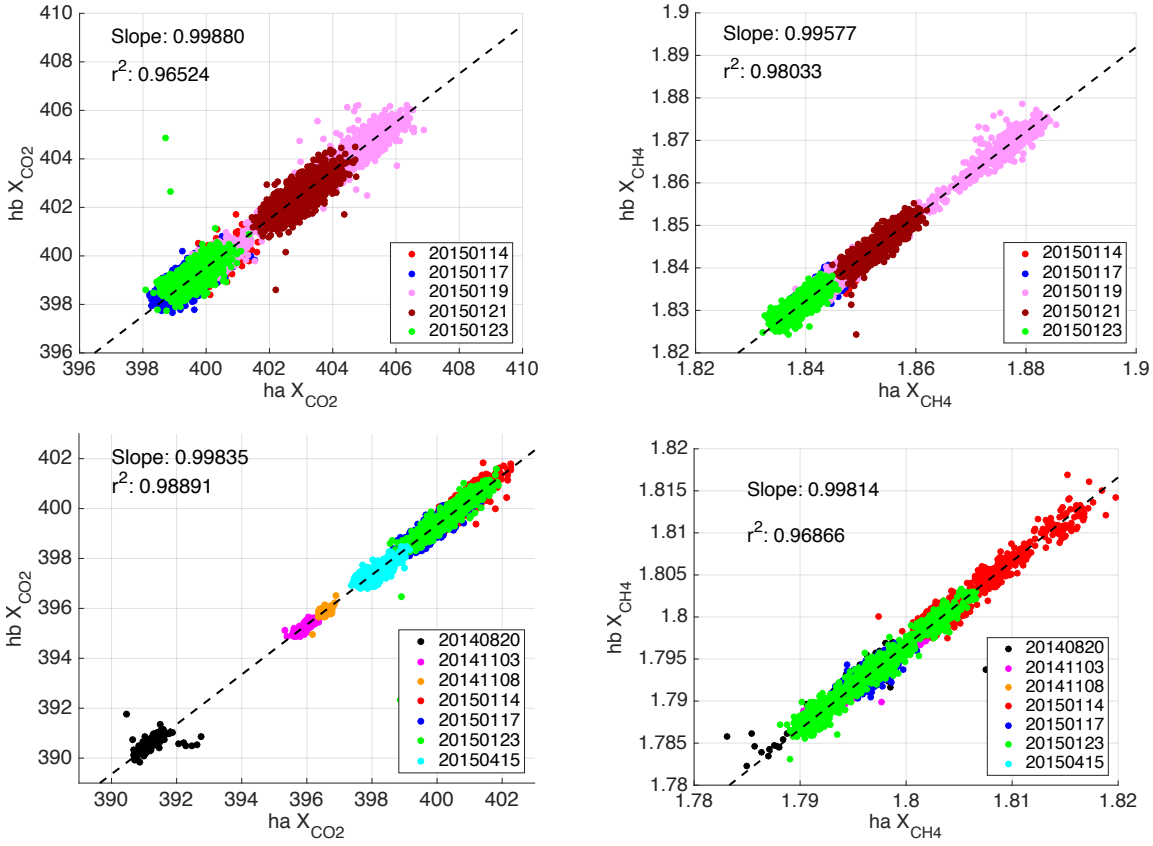

Figure 2. Scatter plots with the slopes representing $\overline{R_G}$ for different days using GFIT (top panels) and PROFFIT retrieval (bottom panels). January measurements are carried out in Pasadena, others in Boston.

The value of $\overline{R_G}$ was very consistent over time for the two Harvard EM27/SUNs, including shipment across the continent and back (Fig. 2). We used two retrieval software systems, GFIT (Wunch et al. (2015)) and PROFFIT (Hase et al. (2004)). $\overline{R_G}$ is 0.99880 for X_{CO_2} with GFIT, 0.99835 with PROFFIT; 0.99577 for X_{CH_4} with GFIT, 0.99814 with PROFFIT. Even though the scaling factors are slightly different for GFIT and PROFFIT, traceable to their specific modeling of the ILS, $\overline{R_G}$ is consistent for different days using one retrieval software. Retrievals for ha have been scaled with $\overline{R_G}$ for the precision assessment above (Sec. 3.1) and for the scientific applications (Sec. 4) below. Scaling factors for pl are shown in Tab.3.

4 Scientific Applications

4.1 Emission of an Area Source

We measured the column-averaged dry-air mole fractions X_{CO_2} and X_{CH_4} simultaneously at locations upwind and downwind of the dairy farms in Chino, California, for several days in January 2015. Field results are shown for *ha, hb*, and pl in Fig. 3.

Atmos. Chem. Phys. Discuss., doi:10.5194/acp-2015-1058, 2016
Manuscript under review for journal Atmos. Chem. Phys.
Published: 17 February 2016

Atmospheric Chemistry and Physics Discussions

Meteorological conditions were particularly favorable on 24 Jan. 2015, with consistent wind directions and wind speeds (∼10 m/s) at both Chino airport (KCNO: 1 km northeast of the downwind station ha) and Ontario airport (KONT: 3 km north of the upwind station hb) (see Fig. 3 (c) panels 3 and 4).

The measured methane enhancement $\Delta X_{\mathrm{CH_4}}$ was notably consistent at ∼2 ppb over 5 hours of measurement (Fig. 3 (c), Tab.1), 10 times larger than our measurement precision using 5 min integration time (see Sec. 3.1). 0.1-0.7 hours from solar noon were not taken into account, because a transient peak was measured at the upwind site.

Winds were more variable on 15 Jan. 2015 (Appendix E), with a consistent period of just ∼1 hour with relatively light wind (∼2 m/s) at the two airports. The observed $\Delta X_{\mathrm{CH_4}}$ was ∼10 ppb (Fig. 3 (d)), a factor of 5 larger than on the 24$^{\mathrm{th}}$, showing inverse proportionality to the wind speed.

We use a simple column model (Jacob (1999)) and literature emission values to *estimate* ΔX_{G} for the dairy farms (area source) and to *verify* our measurements:

$$\Delta X_{\mathrm{G}} = X^d_{\mathrm{G}} - X^u_{\mathrm{G}} = \frac{D}{\overline{U}} \times \frac{E_{\mathrm{G}}}{\mathrm{column}_{\mathrm{dryair}}}, \tag{2}$$

where $\mathrm{column}_{\mathrm{dryair}}$ denotes the column number density of dry air. E_{G} is the mean emission flux $[\mathrm{molec.}/(\mathrm{m^2 s})]$ along the line traversing the area source along the direction sampled at the downwind station, and D is the length of the transect. The frame of reference is the air column, which picks up the emissions of gas G from the dairies as the air traverses the farms. The longer the air column travels in the emission field, the larger the difference between the column number densities of the downwind and upwind sites will become. ΔX_{G} is therefore proportional to the residence time $D/\overline{U}$ of the air column, and inversely proportional to the wind speed $\overline{U}$. This simple column model is applicable when the wind direction and speed are consistent across the area, and fluxes are uniform at plume scale.

Our model assumes that air parcels within the air column are transported with a mean velocity $\overline{U}$ in the horizontal direction, which can be estimated using real-time data for the wind speed at the surface. Using Reynolds' decomposition, the time series of horizontal (u) and vertical (w) wind speed are split into a mean part and a turbulent part, i.e.:

$$u(t) = \overline{u} + u_{\mathrm{turb}}(t), \qquad w(t) = \overline{w} + w_{\mathrm{turb}}(t), \tag{3}$$

$$\sigma_u = \sqrt{< u^2_{\mathrm{turb}} >}, \qquad \sigma_w = \sqrt{< w^2_{\mathrm{turb}} >}. \tag{4}$$

σ_u and σ_w are the standard deviations of the turbulent components. We assume the turbulence is horizontally homogeneous (σ_u is independent of location) and isotropic ($\sigma_w = \sigma_u$), and that the mean vertical wind speed $\overline{w}$ is zero. Strictly speaking, $\overline{U}$ denotes the *mass-enhancement-weighted* wind velocity, i.e. $\overline{u}(z)$ weighted with the vertical distribution of the CH_4 molecules emitted from the dairies, denoted as $\mathrm{PDF}_{\Delta \mathrm{CH_4}}(z)$, i.e.

$$\overline{U} = \int_0^\infty \overline{u}(z)\, \mathrm{PDF}_{\Delta \mathrm{CH_4}}(z) dz. \tag{5}$$

Atmos. Chem. Phys. Discuss., doi:10.5194/acp-2015-1058, 2016
Manuscript under review for journal Atmos. Chem. Phys.
Published: 17 February 2016

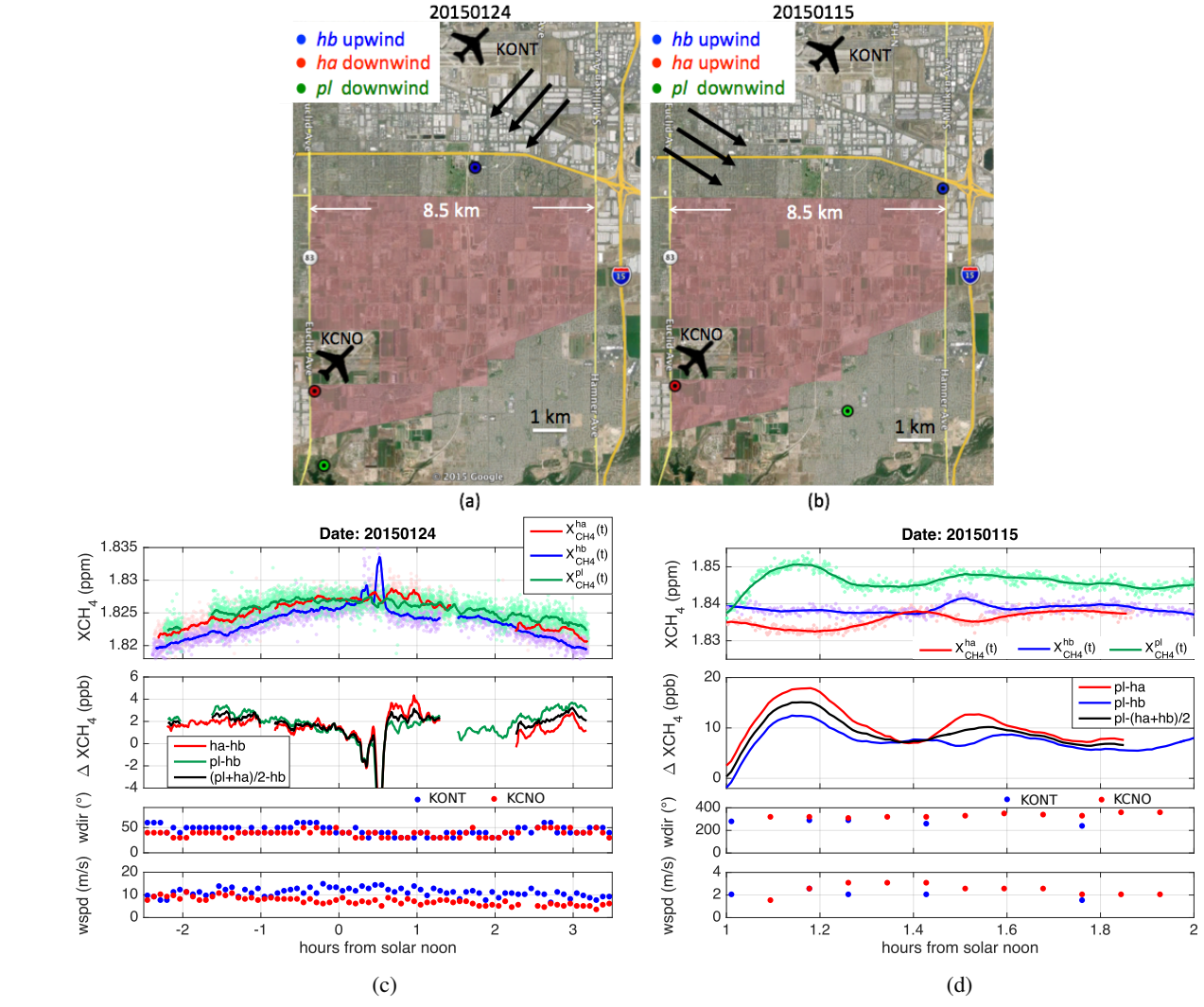

Figure 3. (a) and (b): locations of FTS stations and mean wind directions on 15 and 24 Jan., 2015. (c) and (d): column-averaged DMF measurements at three stations and downwind minus upwind differences (solar zenigh angle $\leq 70^{\circ}$). On 24 Jan., $\Delta X_{\mathrm{CH_4}}$ was steady at $\sim$2 ppb most of the day, 10 times larger than our measurement precision; on 15 Jan., $\Delta X_{\mathrm{CH_4}}(t)$ was $\sim$10 ppb, about 5 times larger than on 24 Jan., showing inverse proportionality to the wind speed. Map provided by Google Earth, Image Landsat, Data SIO, NOAA, U.S. Navy, NGA, and GEBCO.

Atmos. Chem. Phys. Discuss., doi:10.5194/acp-2015-1058, 2016
Manuscript under review for journal Atmos. Chem. Phys.
Published: 17 February 2016

Atmospheric Chemistry and Physics Discussions

Note if $\overline{u}(z) = \text{const.}$, we have $\overline{U} = \overline{u}(z) = \text{const.}$, i.e. $\overline{U}$ is independent of the vertical distribution of the CH_4 molecules being added in the column. However, since the wind speed generally increases with altitude, $\text{PDF}_{\Delta\text{CH}_4}(z)$ needs to be considered for the estimate of $\overline{U}$.

We assume ΔCH_4 is uniformly distributed up to a mixing height z_{emiss} and negligible above, then:

$$\text{PDF}_{\Delta\text{CH}_4}(z) = \begin{cases} \frac{1}{z_{\text{emiss}}}, & 0 \le z \le z_{\text{emiss}}, \\ 0, & z > z_{\text{emiss}}, \end{cases} \tag{6}$$

$$\overline{U} = \frac{1}{z_{\text{emiss}}} \int_0^{z_{\text{emiss}}} \overline{u}(z) dz. \tag{7}$$

We use a 2D random walk model (McCrea and Whipple (1940)) to estimate z_{emiss}, the height to which CH_4 emissions are transported vertically by turbulent flow. The number of the random-walk steps n is given by the ratio between the average transit time of the emission τ_{transit} and the decorrelation time of the turbulent velocities τ_{eddy}, i.e.,

$$n = \frac{\tau_{\text{transit}}}{\tau_{\text{eddy}}} = \frac{D\sigma_w}{2\overline{u}\lambda}. \tag{8}$$

Assuming homogeneous emission, τ_{transit} is approximately $D/2\overline{u}$, with $\overline{u}$ representing the mean speed at the surface. This also corresponds to the transit time of a particle emitted at the center of the field. τ_{eddy} is given by λ/σ_w, where λ denotes the average eddy scale.

On 24 Jan., the mean horizontal wind speed over the entire measurement time is 11.35 m/s at KONT and 7.29 m/s at KCNO with standard deviations of 1.75 m/s and 1.59 m/s, respectively. The wind directions are likewise very consistent over time, with a standard deviation of 8.9° (KONT) and 6.5° (KCNO). The wind speed at 10 m above ground level (agl) is assumed to be the average at the two airports over time, which gives $\overline{u}(10\text{ m}) = 9.3$ m/s with fluctuations $\sigma_u(10\text{ m}) = \sigma_w(10\text{ m}) = 1.7$ m/s. Assuming an average eddy scale of 100 m, the expected value of the height to which CH_4 emissions rise is therefore:

$$z_{\text{emiss}} = \frac{\lambda\sqrt{n}}{\sqrt{2}} = \frac{1}{2}\sqrt{\frac{D\sigma_w(10\text{ m})\lambda}{\overline{u}(10\text{ m})}} = \frac{1}{2}\sqrt{D\,I\,\lambda} \approx 200\text{ m}. \tag{9}$$

According to Taylor's hypothesis (Taylor (1938)), the turbulence intensity $I = \sigma_u/\overline{u}$ should be constant, which indicates z_{emiss} does not depend on $\overline{u}$, but only on the eddy scale λ and the turbulence intensity.

For determining $\overline{U}$ we need to consider the wind profile both in and above the surface layer. The wind follows a roughly logarithmic profile in the surface layer. At the middle portion of the PBL, the wind has typically constant direction and speed (Stull (1988)). Because the surface roughness information is not available, we use the power law to approximate the log wind profile in the surface layer and assume a constant horizontal wind speed above, i.e.,

$$\overline{u}(z) = \begin{cases} \overline{u}(10\text{ m})\,(\frac{z}{10\text{ m}})^{\alpha}, & 0 \le z \le z_{\text{S}}, \\ \overline{u}(10\text{ m})\,(\frac{z_{\text{S}}}{10\text{ m}})^{\alpha}, & z_{\text{S}} < z < z_{\text{PBL}}, \end{cases} \tag{10}$$

Atmos. Chem. Phys. Discuss., doi:10.5194/acp-2015-1058, 2016
Manuscript under review for journal Atmos. Chem. Phys.
Published: 17 February 2016

Atmospheric Chemistry and Physics Discussions

where z_S and z_{PBL} denote the depth of the surface layer and the PBL, respectively. The power law exponent α is approximately $1/7$ for neutral stability conditions (Hsu et al. (1994)). This wind model (Eq. 10) is consistent with the winds reported by aircraft taking off and landing at Ontario airport (see Appendix F).

Inserting Eq. 10 into Eq. 7, we obtain:

$$\overline{U} = \frac{\overline{u}(10\text{ m})}{z_{\text{emiss}}} \left(\int_0^{z_S} \left(\frac{z}{10\text{ m}}\right)^{\alpha} dz + \int_{z_S}^{z_{\text{emiss}}} \left(\frac{z_S}{10\text{ m}}\right)^{\alpha} dz \right)$$
$$= \overline{u}(10\text{ m}) \left(\frac{z_S}{10\text{ m}}\right)^{\alpha} \left(1 - \frac{z_S}{z_{\text{emiss}}} \frac{\alpha}{\alpha+1}\right). \quad (11)$$

Varying z_S in the range of 10 m to z_{emiss}, we obtain $\overline{U}$ in the range of 9.3 to 12.5 m/s, or 10.9 m/s $\pm 15\%$. The lower bound is given by a constant wind speed starting from 10 m agl, and the upper bound assumes a wind profile power law up to the mixing height z_{emiss}.

According to Eq. 2, the uncertainty in calculating E_G from ΔX_G is the sum of the uncertainties in $\overline{U}$ (15%), ΔX_G (0.1‰ precision) and column$_{\text{dryair}}$ (1%). Oxygen column number density is determined as $4.493 \cdot 10^{28}$ molec./m$^2 \pm 1\%$ (Fig.10), accounting for 20.95% of dry air. Therefore, an emission estimate using differential column measurements is dominated by the uncertainty in the transport (i.e. $\overline{U}$), not the differential column measurements themself.

Since the two spectrometers have identical optical setup, spectral resolution, and measuring geometry, their column averaging kernels are very similar, and happen to be close to one at all altitudes (Hedelius et al. (2016)). The uncertainty arising from the differences in averaging kernels is included in the uncertainty in ΔX_G. The sensitivity of X_{CH_4} on surface pressure inputs are discussed in Appendix C.

In Tab.1, the time-averaged ΔX_{CH_4} and their corresponding emission numbers are listed. Measurements between 0.1 and 0.7 hours after solar noon are neglected due to a transient peak measured with hb (Fig. 3).

Configuration	ΔX_{CH_4} (ppb)	E_{CH_4} [molec./(m^{2}s)]	$E_{CH_4,\text{annual}}$ [Gg/yr]
ha - hb	1.8	$5.3 \cdot 10^{17}$ ($\pm 16\%$)	22.3 ($\pm 26\%$)
pl - hb	2.1	$6.1 \cdot 10^{17}$ ($\pm 16\%$)	25.5 ($\pm 26\%$)
$(pl+ha)/2$ - hb	2.1	$6.0 \cdot 10^{17}$ ($\pm 16\%$)	25.3 ($\pm 26\%$)

Table 1. Time-averaged ΔX_{CH_4} for using ha or pl, or ha and pl as downwind stations on 24 Jan. 2015, and their corresponding emission numbers calculated using Eq. 2. ΔX_{CH_4} is rounded to one decimal place, whereas the calculation of E_{CH_4} and $E_{CH_4,\text{annual}}$ are done with full digits. 16% is given by the uncertainties in $\overline{U}$, column$_{\text{dryair}}$, and ΔX_G. Uncertainty in $E_{CH_4,\text{annual}}$ is 16% added with 10% uncertainty in the emission area.

We can compare our measurements to the value of ΔX_{CH_4} derived from literature annual mass emission rates $E_{CH_4,\text{annual}}$ for the dairy farms. Peischl et al. (2013) determined 28 Gg/yr using bottom-up method accounting for enteric fermentation and dry manure management, and 49($\pm 50\%$) Gg/yr using top-down method based on aircraft measurements during the CalNex

Atmos. Chem. Phys. Discuss., doi:10.5194/acp-2015-1058, 2016
Manuscript under review for journal Atmos. Chem. Phys.
Published: 17 February 2016

Atmospheric Chemistry and Physics Discussions

field study. We assume a dairy area ($\text{area}_{\text{emiss}}$) of 50 km$^2 \pm 10\%$ and a constant emission rate across the farm throughout day and night, to convert $E_{\text{CH}_4,\text{annual}}[\text{g/yr}]$ to $E_{\text{CH}_4}[\text{molec.}/(\text{m}^2\text{s})]$. The transect length D is approximated with 8 km, which is the diameter of a circle with 50 km^2 area.

For 24 Jan. 2015,

$$\Delta X_{\text{CH}_4,\text{Exp}} = \frac{D}{\overline{U}} \times \frac{E_{\text{CH}_4,\text{annual}}(\text{Peischl's Number})}{m_{\text{CH}_4} \cdot \text{area}_{\text{emiss}} \cdot N_{\text{s/year}} \cdot \text{column}_{\text{dryair}}}$$
$$= \begin{cases} 2.3 \pm 0.6 \text{ ppb}, & \text{for 28 Gg/yr (bottom-up estimate)}, \\ (4.0 \pm 1.0)(\pm 50\%) \text{ ppb}, & \text{for 49}(\pm 50\%) \text{ Gg/yr (top-down estimate)}, \end{cases}$$

where m_{CH_4} denotes the molecular mass of methane [g/molec.] and $N_{\text{s/year}}$ represents the number of seconds per year.

The observed ΔX_{CH_4}, ~ 2 ppb (Fig. 3(c), Tab. 1), falls in the lower half of the range from Peischl. Our results, and Peischl's top-down estimates, both represent just a few days of data. The difference with Peischl's results using aircraft measurements could be due to seasonal factors, activity levels at the farms, uncertainties in $\overline{U}$, or model errors. Longer deployments with more ancillary data, such as wind profiles, would be needed to refine the result. The differential column measurement using compact FTSs has shown the capability to determine the emission flux when deployed across an area source such as Chino farms.

4.2 Source Characterization Using Ratios of Spatial Column Gradients

The ratio of column gradients can be used to characterize regional emission ratios. For example, Wunch et al. (2009) measured diurnal changes of X_{CH_4}, X_{CO_2}, and X_{CO} (temporal gradient), and used the CO_2 emission inventories from the California Air Resources Board (CARB) and EDGAR (Emission Database for Global Atmospheric Research) to estimate emissions of CH_4 and CO in the South Coast air basin (SCB).

Pasadena is a city within the SCB with heterogeneous CO_2 and CH_4 emissions, from different source types such as transportation, electricity generation, industry, landfills, and gas leaks from natural gas delivery system. The two spectrometers ha and hb were located north (34.2N, 118.13W, 557 m asl) and south (34.11N, 118.14W, 172 m asl) of Pasadena on 27 Jan. 2015. The spatial gradient at time t is given by the difference between the measurements of ha and hb at the same time, i.e. $\Delta X_G(t) = X_G^{hb}(t) - X_G^{ha}(t)$, which is shown in Fig. 4 third panel.

We determine the ratio of *spatial* column gradients $\Delta X_{\text{CH}_4}/\Delta X_{\text{CO}_2}$ across Pasadena, by linear regression of ΔX_{CH_4} and ΔX_{CO_2} data using maximum likelihood estimation (York et al. (2004), see Fig. 5). The determined gradient ratio over the course of the day (7.4 ± 0.1 ppb/ppm) is similar to the emission ratios determined by comparing the daily variations of X_{CH_4} and X_{CO_2} (7.8 ± 0.8 ppb/ppm) reported at a TCCON station (Wunch et al. (2009)) located at JPL (34.2N, 118.2W, 390 m asl), and likewise for the ratio of enhancements obtained by the CLARS-FTS (7.28 ± 0.09 ppb/ppm, Wong et al. (2015)), which compared DMFs from diffuse solar reflectance off a spectralon plate at Mount Wilson (34.22N, 118.06W, 1670 m asl) with those from reflected sunlight from West Pasadena (34.17N, 118.17W).

Atmos. Chem. Phys. Discuss., doi:10.5194/acp-2015-1058, 2016
Manuscript under review for journal Atmos. Chem. Phys.
Published: 17 February 2016

Atmospheric Chemistry and Physics Discussions

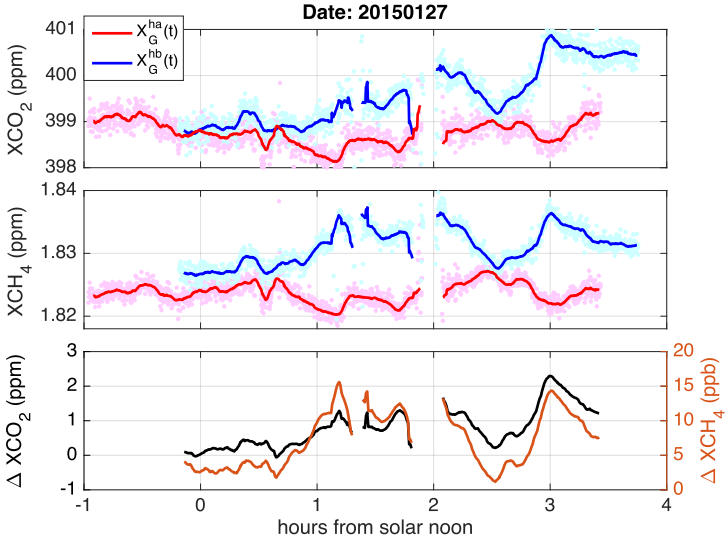

Figure 4. First and second panels: measured X_{CO_2} and X_{CH_4} north (ha) and south (hb) of Pasadena on 27 Jan. with 5 min averaging time. Third panel: ΔX_{CO_2} and ΔX_{CH_4} are temporal correlated and their ratio is determined as 7.4 ppb/ppm, shown in Fig. 5.

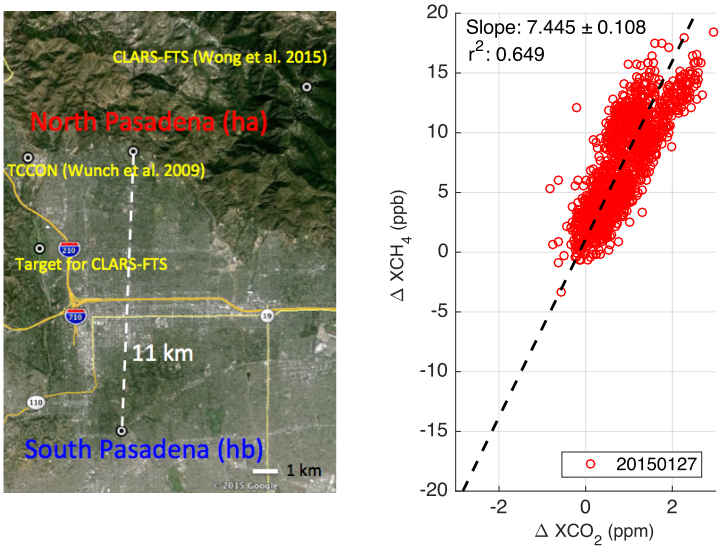

Figure 5. The column gradient ratio across Pasadena is similar to Wunch et al. (2009) using TCCON DMF daily dynamics and very close to the excess ratio determined in Wong et al. (2015), which compared DMFs from diffuse solar reflectance off a spectralon plate at Mount Wilson with those from reflected sunlight from West Pasadena. Map provided by Google Earth, Image Landsat, Data SIO, NOAA, U.S. Navy, NGA, and GEBCO.

By coloring the gradient ratios per hour (Fig. 6), we observe a difference in the gradient ratios between noon (9.8 ± 0.2 ppb/ppm) and afternoon time (6.8 ± 0.1 ppb/ppm), with both regression curves passing essentially through the origins. We

Atmos. Chem. Phys. Discuss., doi:10.5194/acp-2015-1058, 2016
Manuscript under review for journal Atmos. Chem. Phys.
Published: 17 February 2016

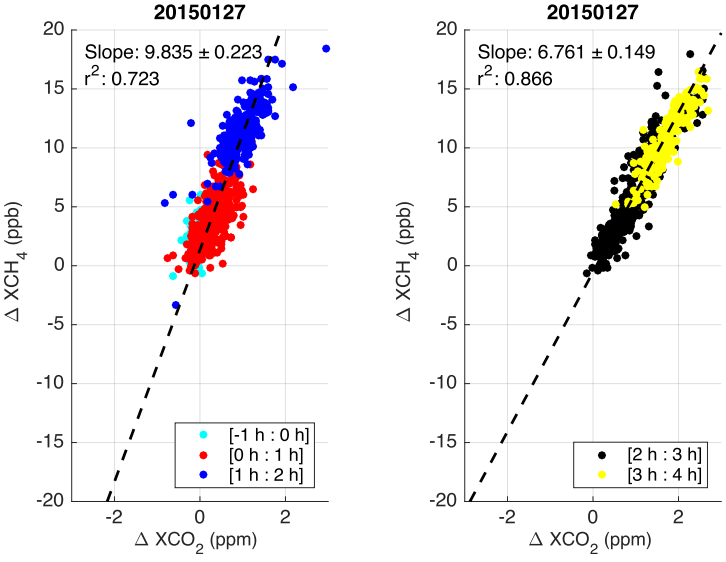

Figure 6. Column gradient ratio measured across Pasadena colored by hours. Both regression curves essentially pass through the origins that are shown as crosses.

determined a higher $\Delta X_{CO_2}/\Delta X_{CH_4}$ ratio in the afternoon than the noon time, which can be caused by more traffic emissions in the basin. The lagged cross covariance between ΔX_{CO_2} and ΔX_{CH_4} peaks at zero lag, and the peak value is interestingly higher than the peak value of the cross covariance function between X_{CO_2} and X_{CH_4} at individual sites (Fig. 13 in Appendix G), which suggests the spatial gradient is also sensitive to the emissions between the two sites.

The Pasadena study confirms that sources of CH_4 are surprisingly large from SCB, as reported by previous papers using aircraft and TCCON data (Wunch et al. (2009); Wennberg et al. (2012); Peischl et al. (2013)). The capability of the column gradient ratio measurements for determining emission ratios is illustrated here.

4.3 Short-Term Variations

We observed short-term variations in side by side measurements at Caltech and Harvard. These fluctuations are captured by both instruments simultaneously, representing geophysical phenomena, not noise as might be assumed. The high frequency temporal structure ($\sim$ 5-10 min Full Width at Half Maximum) can be caused by emissions not well mixed within the boundary layer ("plumes"), or by turbulence across the top of the ML, or by intrusions of a sea breeze front that introduces a different volume of air to the column, etc.

In Fig. 7 we show, as an example, side by side measurements at Caltech. Short-term variations in X_{CO_2} as large as 1 ppm are observed between 19:30 and 23:00 UTC. These features are only present in X_{CO_2}, not in X_{CH_4}, and are likely due to excess CO_2 emissions from a 12.5 MW natural gas power plant located $\sim$ 200 m to the south-southwest and/or a 0.1 MW solid oxide fuel cell $\sim$ 20 m to the northwest. Note that, because the co-located TCCON spectrometer samples at a lower rate, these variations are not well resolved in the TCCON data (Wennberg et al. (2014)).

Atmos. Chem. Phys. Discuss., doi:10.5194/acp-2015-1058, 2016
Manuscript under review for journal Atmos. Chem. Phys.
Published: 17 February 2016

Atmospheric Chemistry and Physics Discussions

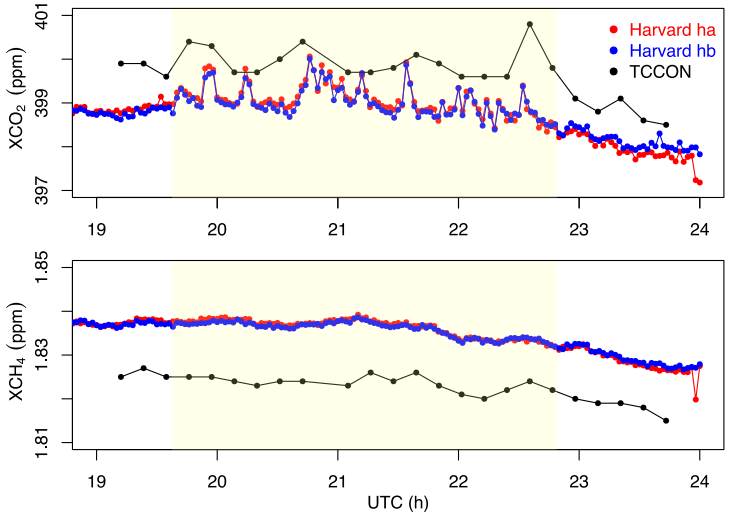

Figure 7. Side by side measurements on the roof of Caltech (17 Jan. 2015). Both EM27/SUN spectrometers (2 min block-average) captured short-term variations of X_{CO_2} signal ($\sim$ 1 ppm corresponds to 2.5‰ relative). TCCON spectrometer does not resolve these short-term variation due to the low measurement rate.

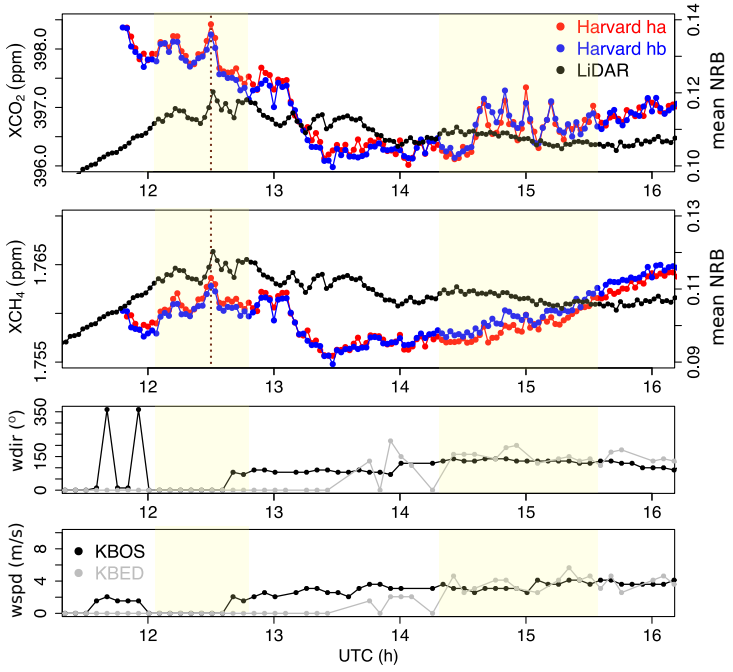

Figure 8. Short-term variations in X_{CO_2} and X_{CH_4} observed on the roof of Harvard Science Center by *ha* and *hb* (date: 16 April 2015; 2 min mean block average). A LiDAR metric of the thickness of the PBL (mean NRB 0-1.5 km agl) from a nearby site (Boston University, 3 km to the south-southeast of our site) is overlaid on top. The NRB signal is positively correlated with the short-term variations of the FTS measurements at 12-13 UTC.

Atmos. Chem. Phys. Discuss., doi:10.5194/acp-2015-1058, 2016
Manuscript under review for journal Atmos. Chem. Phys.
Published: 17 February 2016

Atmospheric Chemistry and Physics Discussions

Fig. 8 shows another example in Boston where X_{CO_2} and X_{CH_4} vary together by approximately the same relative amount (1-2‰) at 12-13 UTC, also correlated with changes ($\sim$ 10%) in the mean relative backscatter (NRB) measured from our LiDAR station 3 km away (Appendix H). The wind measurements at Boston Logan International Airport (KBOS), showing easterly winds during that time period, differ from New Bedford Regional Airport (KBED), indicating a sea breeze event that likely generates wind shear and turbulence across the top of the ML. The depth of PBL undergoes short-term variations that are also visible in the LiDAR data at 12:30 UTC. In this case, the column-averaged DMFs vary because the proportion of PBL air in the whole column changes. Also the sea breeze circulation pushes a different volume of air through the column, which could result in a sporadic jump of X_{CO_2} and X_{CH_4}. The short-term variation of X_{CO_2} at 14-16 UTC is not observed in X_{CH_4} and the LiDAR data. It is probably caused by CO_2 plumes within the PBL, similar to what we observed at Caltech and shown in Fig. 7.

The short-term variation helps us to understand the limitation of sampling using column measurements, which is relevant to the gradient determination and to satellite data. It is highly desirable to avoid aliasing these variations, and to characterize, model and/or measure the influences that cause these variations.

5 Conclusions

In this paper we demonstrated how to design observations of, and interpret, spatial gradients of column-averaged dry-air mole fractions for trace gases (CO_2, CH_4). We showed that the differential column methodology can be applied to the urban source problem and to other regional source-sink determinations.

We made extensive side-by-side measurements using two EM27/SUNs, in Boston and Pasadena, over many months. The differential system has a precision of 0.1‰ for both X_{CO_2} and X_{CH_4} according to the Allan variance analysis when using an optimum integrating time of 10 min. The system is very stable in measuring column concentrations over time and after relocation across the continent.

We tested the gradient measurement and its sensitivity to emission sources, by measuring the downwind minus upwind column gradient ΔX_{CH_4} across dairy farms in the Chino area. The signal-to-noise ratio for the gradient determination was greater than 10, and the observed column gradients were consistent with values derived from the emission numbers given by Peischl et al. (2013). Spatial column gradient ratios $\Delta X_{CH_4}/\Delta X_{CO_2}$ were measured across Pasadena within South Coast air basin, with values consistent with emission ratios from the literature.

We observed significant short-term variations of X_{CH_4} and X_{CO_2}, and showed that they are not noise or variation of optical path length, but represent atmospheric phenomena. These measurements provide useful information for measuring pollution plumes, turbulences across the top of the mixed layer and airmass variability within the PBL given by e.g. sea breeze circulation.

Overall, this paper helps to establish a range of new applications for compact solar-tracking Fourier transform spectrometers, and shows the capability of differential column measurements for determining urban emissions. By accurately measuring the *differences* in the integrated column amounts across local and regional sources, we directly observe the mass loading of the atmosphere due to the influence of emissions in the intervening locale. The inference of the source strength is much more direct

Atmos. Chem. Phys. Discuss., doi:10.5194/acp-2015-1058, 2016
Manuscript under review for journal Atmos. Chem. Phys.
Published: 17 February 2016

Atmospheric Chemistry and Physics Discussions

than inversion modeling using only surface concentrations, and less subject to errors associated with small-scale transport phenomena. The advent of compact, robust solar viewing spectrometers opens up myriad applications not hitherto pursued.

Appendix A: Instrument Line Function Parameters

The measured spectrum is a convolution between the atmospheric spectrum and instrument line shape in the frequency domain ILS(ν). In the ideal case, ILS(ν) is a delta function, which corresponds to a constant modulation efficiency for all optical path length differences. However, in practice, ILS(ν) is broader than a delta impulse, caused by the spectrometer's finite optical pathlength, finite aperture size and also misalignment of the interferometer. The ILS in the interferogram domain can be approximated using a simple model that assumes a linear decay of the modulation efficiency with increasing optical pathlength difference and a constant phase error (Hase et al. (1999)).

We estimated the ILS parameters of both spectrometers with an experimental setup, similar as described in Frey et al. (2015) and determined the modulation efficiency at maximum optical path length (OPD_{max}) and phase error using the simple model implemented in the LINEFIT software (Hase et al. (1999)). Matlab scripts for automation purposes have been developed and can be obtained from the corresponding author.

Even though the measured ILS parameters are different for the two spectrometers due to the different internal alignment, the ILS of each single instrument is consistent over time and after relocation of the instrument across the contiguous US (see Tab. 2).

Boston		
Instrument	modulation efficiency at OPD_{max}	phase error (rad)
ha	0.975	$-3{\cdot}10^{-3}$
hb	0.988	$5{\cdot}10^{-3}$
Pasadena		
Instrument	modulation efficiency at OPD_{max}	phase error (rad)
ha	0.977	$-2{\cdot}10^{-3}$
hb	0.991	$4{\cdot}10^{-3}$

Table 2. Modulation efficiency and phase error determined for EM27/SUN ha and hb in Boston and Pasadena.

Appendix B: Scaling factors for ha and pl

Tab. 3 shows the scaling factors for ha and pl to match hb measurements, determined by linear regressions of the side-by-side measurements on the roof.

Atmos. Chem. Phys. Discuss., doi:10.5194/acp-2015-1058, 2016
Manuscript under review for journal Atmos. Chem. Phys.
Published: 17 February 2016

Atmospheric Chemistry and Physics Discussions

Instrument	$\overline{R_{CH_4}}$	$\overline{R_{CO_2}}$	$\overline{R_{O_2}}$
ha	0.99577	0.99880	1.00848
pl	1.00093	0.99930	0.99713

Table 3. Scaling factors for ha and pl to match hb, for X_{CH_4}, X_{CO_2} and the oxygen column number density measurements.

The linear models applied are:

$$X^{hb}_{CH_4} = X^{ha}_{CH_4} \cdot \overline{R^{ha}_{CH_4}}, \qquad X^{hb}_{CH_4} = X^{pl}_{CH_4} \cdot \overline{R^{pl}_{CH_4}}, \tag{B1}$$

$$X^{hb}_{CO_2} = X^{ha}_{CO_2} \cdot \overline{R^{ha}_{CO_2}}, \qquad X^{hb}_{CO_2} = X^{pl}_{CO_2} \cdot \overline{R^{pl}_{CO_2}}, \tag{B2}$$

$$\text{column}^{hb}_{O_2} = \text{column}^{ha}_{O_2} \cdot \overline{R^{ha}_{O_2}}, \qquad \text{column}^{hb}_{O_2} = \text{column}^{pl}_{O_2} \cdot \overline{R^{pl}_{O_2}}. \tag{B3}$$

Appendix C: Pressure Inputs for 20150124 Retrievals

Surface pressure P_{surf} is a main input for the GFIT retrieval, to derive the site pressure altitude for each spectrum (Wunch et al. (2011)). Inaccurate pressure measurements will introduce errors in the computed widths of the gas absorption lines, i.e. pressure broadening, and therefore the fitted volume mixing ratio scale factors (Wunch et al. (2011)) will be inadequate, with a biased DMF as a result.

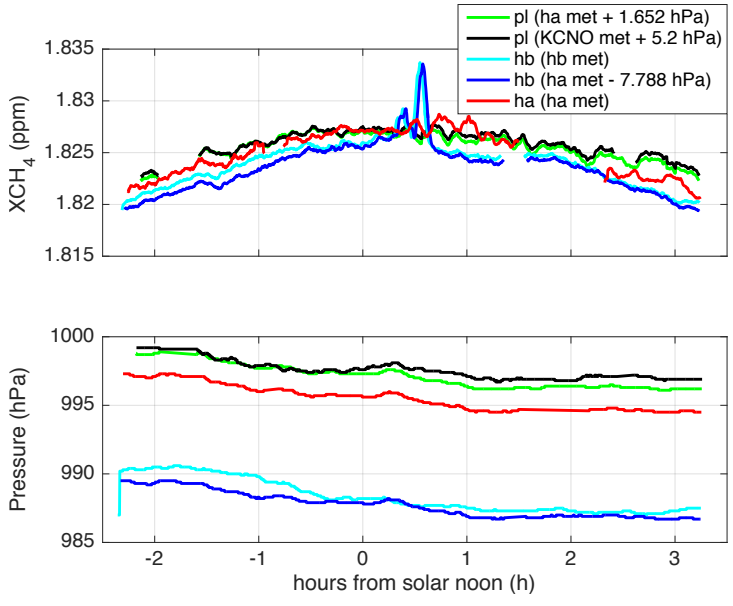

Figure 9. Surface pressure inputs (lower panel) and the corresponding X_{CH_4} retrieval results averaged for 5 min (upper panel). For Fig. 3(c) and the simple column model calculations, ha, hb and pl retrievals with the surface pressure inputs based on ha pressure measurements are used (red, blue and green curves).

Atmos. Chem. Phys. Discuss., doi:10.5194/acp-2015-1058, 2016
Manuscript under review for journal Atmos. Chem. Phys.
Published: 17 February 2016

Atmospheric Chemistry and Physics Discussions

On 24 Jan., the surface pressure measurement at pl site failed, therefore we assess P_{surf}^{pl} using pressure measurements at the closest FTS station ha and the nearby airport KCNO. We assume hydrostatic equilibrium and a 1.18 hPa pressure difference per 10 m altitude difference. We derived ΔP_{surf} using the altitude difference between pl and ha, as well as pl and KCNO airport, and these two methods provide very similar results (Fig. 9). For the simple column model calculations, the retrieval with P_{surf}^{pl} computed using P_{surf}^{ha} and 1.652 hPa offset is used.

For consistency and a fair comparison with ha and pl, hb spectra are also retrieved with the surface pressure input calculated using P_{surf}^{ha} and a negative 7.788 hPa offset, given by 66 m altitude difference. The strong wind could affect the pressure measurement (Bernoulli's equation), which might be the reason for why hb retrieval using its on-site pressure measurements slightly diverges from the result using the pressure data derived from ha met (blue curve in Fig. 9).

Appendix D: Oxygen Column Measurements on 24 Jan. 2015

Fig. 10 shows the ha, hb and pl measurements of oxygen column number densities. The deviations between three sites and the variations during the course of the day are given by the differences in atmospheric surface pressures and water column number densities. ha and pl measurements are scaled with the factors shown in Tab. 3 third column.

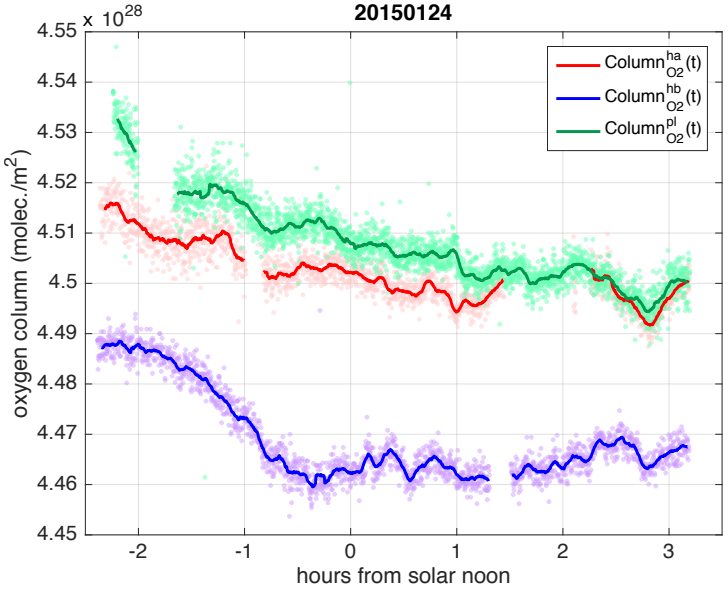

Figure 10. Oxygen column number densities measured by ha, hb and pl on 24 Jan. 2015.

Atmos. Chem. Phys. Discuss., doi:10.5194/acp-2015-1058, 2016
Manuscript under review for journal Atmos. Chem. Phys.
Published: 17 February 2016

Atmospheric Chemistry and Physics Discussions

Appendix E: Gradient Measurement on 15 Jan. 2015

Fig. 11 shows the measurements of X_{CH_4}, ΔX_{CH_4}, wind speeds, and wind directions for the entire day. For verifying the simple column model, we select the time period between 1 and 2 hours after solar noon with relatively consistent wind speeds and directions at KONT and KCNO. The data for the selected time window is shown in Fig. 3 (d).

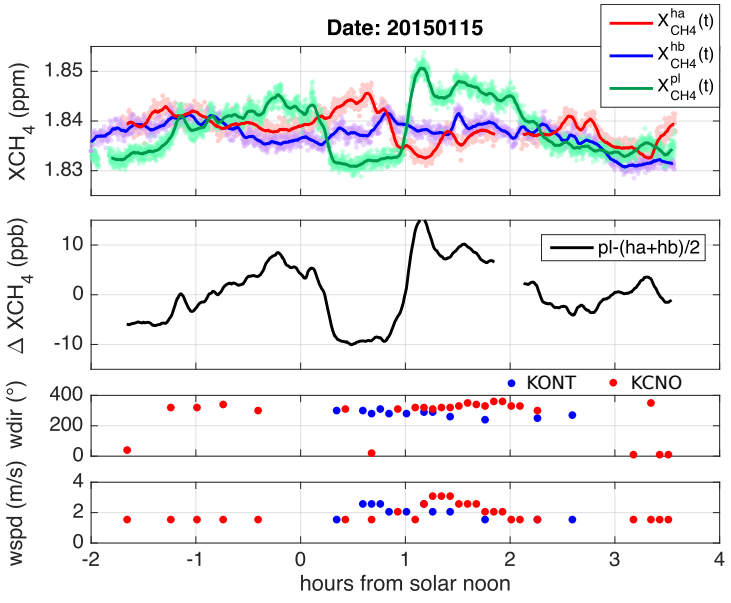

Figure 11. The whole day measurements on 15 Jan. 2015 for ha, hb and pl. We neglect the wind measurements with zero wind speed. Gradient measurements between 1 and 2 hours after solar noon are selected (Fig. 3 (d)) because of the relatively consistent wind speeds and directions at KONT and KCNO.

Appendix F: ACARS aircraft profile data on 24 Jan. 2015

In Fig. 12 we show the automated aircraft reports on profiles measured when taking off and landing at Ontario airport (MADIS ACARS profile data) and the automated surface observing system (ASOS) data, to examine the validity of the wind model described in Eq. 10. Two profiles were captured during the FTS measurement period, where only data above 2000 m agl are available. For plotting the model, we assume the surface layer height is $z_S = 100$ m and the power law exponent $\alpha = 1/7$.

The potential temperature profiles during the FTS measurements and 2-3 hours after are also shown in Fig. 12 third and fourth panels. For the calculations we use the ACARS temperature profiles and the pressure profiles derived from the barometric formula, the ASOS sea level pressure data and a scale height of 7.4 km. Within the middle portion of the ML, the temperature profile follows adiabatic lapse rate, i.e. the potential temperature is nearly constant with height. This behavior is observed between roughly 200 m and 800 m agl at 2-3 hours after the measurement period. During the FTS measurement period, the

Atmos. Chem. Phys. Discuss., doi:10.5194/acp-2015-1058, 2016
Manuscript under review for journal Atmos. Chem. Phys.
Published: 17 February 2016

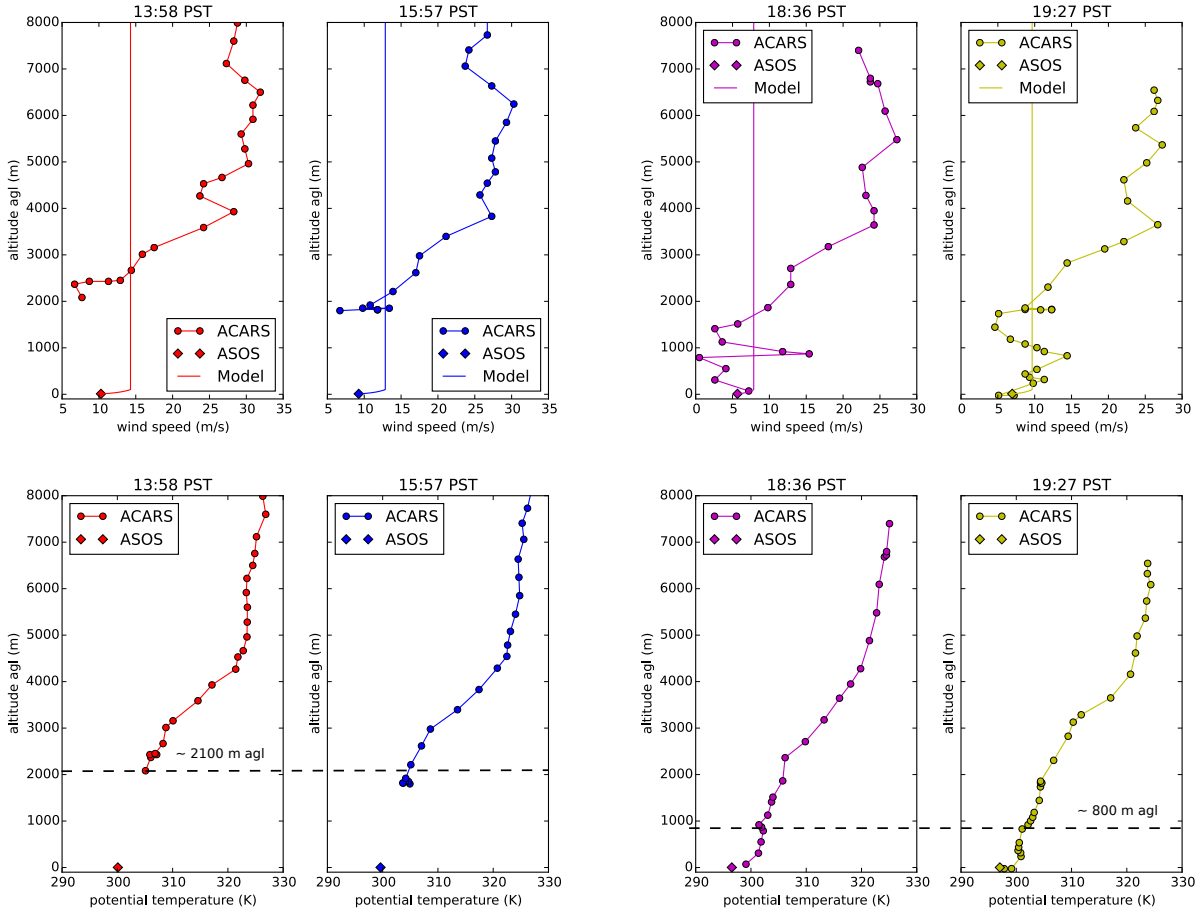

Figure 12. Vertical profile of the horizontal wind speed measurements and the calculated potential temperature profiles, at Ontario airport during (13:58 PST and 15:57 PST) and after the FTS measurements (18:36 PST and 19:27 PST).

airplanes capture data above 2100 m agl where the adiabatic process is not observed. Therefore the PBL height is determined to be in the range of 800 to 2100 m agl. The surface layer is typically the bottom 10% of the PBL.

Appendix G: Cross covariance function between the X_{CH_4} and X_{CO_2} on 27 Jan. 2015

The lagged cross covariance between X_{CH_4} and X_{CO_2} for individual sites measured with *ha* and *hb*, and between ΔX_{CH_4} and ΔX_{CO_2} are shown in Fig. 13.

Atmos. Chem. Phys. Discuss., doi:10.5194/acp-2015-1058, 2016
Manuscript under review for journal Atmos. Chem. Phys.
Published: 17 February 2016

Atmospheric Chemistry and Physics Discussions

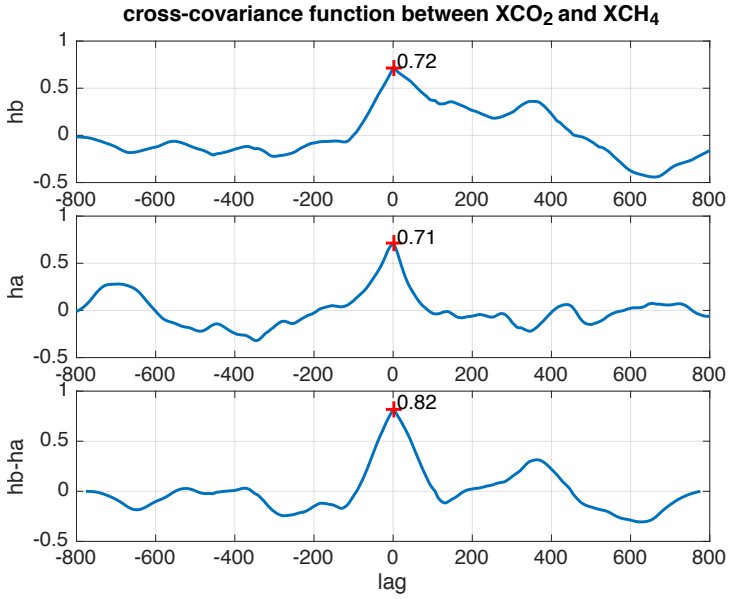

Figure 13. The cross covariance function (mean-removed cross correlation) between $X_{\mathrm{CH_4}}$ and $X_{\mathrm{CO_2}}$ for individual sites measured with *ha* and *hb* are shown in first and second panels. The lagged cross covariance between $\Delta X_{\mathrm{CH_4}}$ and $\Delta X_{\mathrm{CO_2}}$ (third panel) has a larger value at zero lag compared to the first and second panels.

Appendix H: LiDAR measurement in Boston

Fig. 14 shows the normalized relative backscatter (NRB) signal recorded using a Mini Micro Pulse LiDAR (MiniMPL from company Sigma Space) on the roof of the Boston University (BU) on 16 April 2015. We integrate the NRB signal vertically from 0 to 1.5 km to obtain the mean NRB. The time series of the mean NRB together with our FTS measurements are shown in Fig. 8.

Atmos. Chem. Phys. Discuss., doi:10.5194/acp-2015-1058, 2016
Manuscript under review for journal Atmos. Chem. Phys.
Published: 17 February 2016

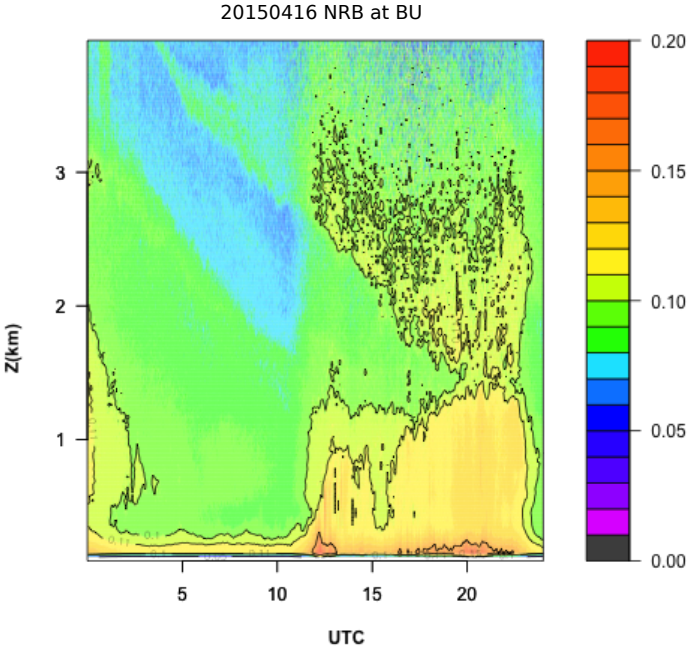

Figure 14. LiDAR measurement on the roof of Boston University on 20150416.

Acknowledgements. We thank Bruce Daube, John Budney for the preparation of the measurement campaign in Chino and Pasadena, and for building the weather stations and the enclosures for the spectrometers. We thank Frank Hase for help with the PROFFIT retrieval software, Matthias Frey for instructions on the ILS measurements, and Matthäus Kiel for the Calpy software. We thank Yanina Barrera for the LiDAR data, and Frank Hase, Kelly Chance, Christoph Gerbig, Bruce Daube, John Budney, Bill Munger, Rachel Chang, and Kathryn McKain for fruitful discussions. Funding for this study was provided by the National Science Foundation through Major Research Instrumentation Award 1337512 "Acquisition of Mesoscale Network of Surface Sensors and Solar-tracking Spectrometers". Jia Chen was partly supported by Technische Universität München - Institute for Advanced Study, funded by the German Excellence Initiative and the European Union Seventh Framework Programme under grant agreement n° 291763. Harrison Parker and Manvendra K. Dubey (Los Alamos National Laboratory) acknowledge NASA's Carbon Monitoring Program for funding the EM27/SUN application development.

Atmos. Chem. Phys. Discuss., doi:10.5194/acp-2015-1058, 2016
Manuscript under review for journal Atmos. Chem. Phys.
Published: 17 February 2016

Atmospheric Chemistry and Physics Discussions

References

Allan, D. W.: Statistics of atomic frequency standards, Proceedings of the IEEE, 54, 221–230, 1966.

Bréon, F., Broquet, G., Puygrenier, V., Chevallier, F., Xueref-Remy, I., Ramonet, M., Dieudonné, E., Lopez, M., Schmidt, M., Perrussel, O., et al.: An attempt at estimating Paris area CO_2 emissions from atmospheric concentration measurements, Atmospheric Chemistry and Physics, 15, 1707–1724, 2015.

Chang, R. Y.-W., Miller, C. E., Dinardo, S. J., Karion, A., Sweeney, C., Daube, B. C., Henderson, J. M., Mountain, M. E., Eluszkiewicz, J., Miller, J. B., et al.: Methane emissions from Alaska in 2012 from CARVE airborne observations, Proceedings of the National Academy of Sciences, 111, 16 694–16 699, 2014.

Crisp, D., Miller, C. E., and DeCola, P. L.: NASA Orbiting Carbon Observatory: measuring the column averaged carbon dioxide mole fraction from space, Journal of Applied Remote Sensing, 2, 023 508–023 508, 2008.

Frankenberg, C., Pollock, R., Lee, R., Rosenberg, R., Blavier, J.-F., Crisp, D., O'Dell, C., Osterman, G., Roehl, C., Wennberg, P., et al.: The Orbiting Carbon Observatory (OCO-2): spectrometer performance evaluation using pre-launch direct sun measurements., Atmospheric Measurement Techniques, 8, 2015.

Frey, M., Hase, F., Blumenstock, T., Groß, J., Kiel, M., Mengistu Tsidu, G., Schäfer, K., Sha, M., and Orphal, J.: Calibration and instrumental line shape characterization of a set of portable FTIR spectrometers for detecting greenhouse gas emissions, Atmospheric Measurement Techniques, 8, 3047–3057, 2015.

Fu, D., Pongetti, T., Blavier, J.-F., Crawford, T., Manatt, K., Toon, G., Wong, K., and Sander, S.: Near-infrared remote sensing of Los Angeles trace gas distributions from a mountaintop site, Atmospheric Measurement Techniques, 7, 713–729, 2014.

Gisi, M., Hase, F., Dohe, S., and Blumenstock, T.: Camtracker: a new camera controlled high precision solar tracker system for FTIR-spectrometers, Atmospheric Measurement Techniques, 4, 47–54, doi:10.5194/amt-4-47-2011, 2011.

Gisi, M., Hase, F., Dohe, S., Blumenstock, T., Simon, A., and Keens, A.: XCO_2-measurements with a tabletop FTS using solar absorption spectroscopy, Atmospheric Measurement Techniques, 5, 2969–2980, 2012.

Hase, F., Blumenstock, T., and Paton-Walsh, C.: Analysis of the instrumental line shape of high-resolution Fourier transform IR spectrometers with gas cell measurements and new retrieval software, Applied Optics, 38, 1999.

Hase, F., Hannigan, J., Coffey, M., Goldman, A., Höpfner, M., Jones, N., Rinsland, C., and Wood, S.: Intercomparison of retrieval codes used for the analysis of high-resolution, ground-based FTIR measurements, Journal of Quantitative Spectroscopy and Radiative Transfer, 87, 25–52, 2004.

Hase, F., Frey, M., Blumenstock, T., Groß, J., Kiel, M., Kohlhepp, R., Mengistu Tsidu, G., Schäfer, K., Sha, M., and Orphal, J.: Application of portable FTIR spectrometers for detecting greenhouse gas emissions of the major city Berlin, Atmospheric Measurement Techniques, 8, 3059–3068, 2015.

Hedelius, J. K., Viatte, C., Wunch, D., C., R., Toon, G. C., Chen, J., Jones, T., Wofsy, S. C., Franklin, J. E., Parker, H., Dubey, M., and Wennberg, P. O.: Assessment of errors and biases in Xgas retrieved from a low resolution spectrometer (EM27/SUN), submitted to Atmospheric Measurement Techniques, amt-2016-39, initial submission, 2016.

Hsu, S., Meindl, E. A., and Gilhousen, D. B.: Determining the power-law wind-profile exponent under near-neutral stability conditions at sea, Journal of Applied Meteorology, 33, 757–765, 1994.

Jacob, D.: Introduction to atmospheric chemistry, Princeton University Press, 1999.

Atmos. Chem. Phys. Discuss., doi:10.5194/acp-2015-1058, 2016
Manuscript under review for journal Atmos. Chem. Phys.
Published: 17 February 2016

Kort, E. A., Frankenberg, C., Miller, C. E., and Oda, T.: Space-based observations of megacity carbon dioxide, Geophysical Research Letters, 39, 2012.

Kort, E. A., Frankenberg, C., Costigan, K. R., Lindenmaier, R., Dubey, M. K., and Wunch, D.: Four corners: The largest US methane anomaly viewed from space, Geophysical Research Letters, 41, 6898–6903, 2014.

Lindenmaier, R., Dubey, M. K., Henderson, B. G., Butterfield, Z. T., Herman, J. R., Rahn, T., and Lee, S.-H.: Multiscale observations of CO_2, $^{13}CO_2$, and pollutants at Four Corners for emission verification and attribution, Proceedings of the National Academy of Sciences, 111, 8386–8391, 2014.

McCrea, W. and Whipple, F.: Random Paths in Two and Three Dimensions., Proceedings of the Royal Society of Edinburgh, 60, 281–298, 1940.

McKain, K., Wofsy, S. C., Nehrkorn, T., Eluszkiewicz, J., Ehleringer, J. R., and Stephens, B. B.: Assessment of ground-based atmospheric observations for verification of greenhouse gas emissions from an urban region, Proceedings of the National Academy of Sciences, 109, 8423–8428, 2012.

Mellqvist, J., Samuelsson, J., Johansson, J., Rivera, C., Lefer, B., Alvarez, S., and Jolly, J.: Measurements of industrial emissions of alkenes in Texas using the solar occultation flux method, Journal of Geophysical Research: Atmospheres (1984–2012), 115, 2010.

Peischl, J., Ryerson, T. B., Brioude, J., Aikin, K. C., Andrews, A. E., Atlas, E., Blake, D., Daube, B. C., de Gouw, J. A., Dlugokencky, E., Frost, G. J., Gentner, D. R., Gilman, J. B., Goldstein, A. H., Harley, R. A., Holloway, J. S., Kofler, J., Kuster, W. C., Lang, P. M., Novelli, P. C., Santoni, G. W., Trainer, M., Wofsy, S. C., and Parrish, D. D.: Quantifying sources of methane using light alkanes in the Los Angeles basin, California, Journal of Geophysical Research: Atmospheres, 118, 4974–4990, 2013.

Picarro: Datasheet G2301 CRDS Analyzer for CO_2, CH_4, H_2O Measurements in Air, https://picarro.app.box.com/s/5er36ac0ncmy1eruxge1p231cy00sl7k, 2015a.

Picarro: Datasheet G2401 CRDS Analyzer for CO_2, CO, CH_4, H_2O in Air, https://picarro.app.box.com/s/vfh80atc42tnq04t4a996t8sestqov9x, 2015b.

Stremme, W., Ortega, I., and Grutter, M.: Using ground-based solar and lunar infrared spectroscopy to study the diurnal trend of carbon monoxide in the Mexico City boundary layer, Atmospheric Chemistry and Physics, 9, 8061–8078, 2009.

Stremme, W., Grutter, M., Rivera, C., Bezanilla, A., Garcia, A., Ortega, I., George, M., Clerbaux, C., Coheur, P.-F., Hurtmans, D., et al.: Top-down estimation of carbon monoxide emissions from the Mexico Megacity based on FTIR measurements from ground and space, Atmospheric Chemistry and Physics, 13, 1357–1376, 2013.

Stull, R. B.: An introduction to boundary layer meteorology, vol. 13, Springer Science & Business Media, 1988.

Taylor, G. I.: The spectrum of turbulence, in: Proceedings of the Royal Society of London A: Mathematical, Physical and Engineering Sciences, vol. 164, pp. 476–490, The Royal Society, 1938.

Té, Y., Dieudonné, E., Jeseck, P., Hase, F., Hadji-Lazaro, J., Clerbaux, C., Ravetta, F., Payan, S., Pépin, I., Hurtmans, D., et al.: Carbon monoxide urban emission monitoring: A ground-based FTIR case study, Journal of atmospheric and oceanic technology, 29, 911–921, 2012.

UNHabitat: Global Report on Human Settlement 2011, http://mirror.unhabitat.org/downloads/docs/E_Hot_Cities.pdf, visited 12 Nov. 2015, 2011.

Veefkind, J., Aben, I., McMullan, K., Förster, H., De Vries, J., Otter, G., Claas, J., Eskes, H., De Haan, J., Kleipool, Q., et al.: TROPOMI on the ESA Sentinel-5 Precursor: A GMES mission for global observations of the atmospheric composition for climate, air quality and ozone layer applications, Remote Sensing of Environment, 120, 70–83, 2012.

Atmos. Chem. Phys. Discuss., doi:10.5194/acp-2015-1058, 2016
Manuscript under review for journal Atmos. Chem. Phys.
Published: 17 February 2016

Wennberg, P. O., Mui, W., Wunch, D., Kort, E. A., Blake, D. R., Atlas, E. L., Santoni, G. W., Wofsy, S. C., Diskin, G. S., Jeong, S., et al.: On the sources of methane to the Los Angeles atmosphere, Environmental science & technology, 46, 9282–9289, 2012.

Wennberg, P. O., Wunch, D., Roehl, C., Blavier, J.-F., Toon, G. C., and Allen, N.: TCCON data from California Institute of Technology, Pasadena, California, USA, Release GGG2014R1, TCCON data archive, hosted by the Carbon Dioxide Information Analysis Center, Oak Ridge National Laboratory, Oak Ridge, Tennessee, U.S.A., doi:10.14291/tccon.ggg2014.pasadena01.R1/1182415, 2014.

Werle, P., Mücke, R., and Slemr, F.: The limits of signal averaging in atmospheric trace-gas monitoring by tunable diode-laser absorption spectroscopy (TDLAS), Applied Physics B, 57, 131–139, 1993.

WHO: http://www.who.int/gho/urban_health/situation_trends/urban_population_growth_text, visited on 28 Oct. 2015, 2014.

Wong, K., Fu, D., Pongetti, T., Newman, S., Kort, E., Duren, R., Hsu, Y.-K., Miller, C., Yung, Y., and Sander, S.: Mapping CH_4: CO_2 ratios in Los Angeles with CLARS-FTS from Mount Wilson, California, Atmospheric Chemistry and Physics, 15, 241–252, 2015.

Wunch, D., Wennberg, P. O., Toon, G. C., Keppel-Aleks, G., and Yavin, Y. G.: Emissions of greenhouse gases from a North American megacity, Geophysical Research Letters, 36, L15 810, 2009.

Wunch, D., Toon, G. C., Blavier, J. F., Washenfelder, R. A., Notholt, J., Connor, B. J., Griffith, D. W., Sherlock, V., and Wennberg, P. O.: The total carbon column observing network, Philos Trans A Math Phys Eng Sci, 369, 2087–112, 2011.

Wunch, D., Toon, G. C., Sherlock, V., Deutscher, N. M., Liu, X., Feist, D. G., and Wennberg, P. O.: The Total Carbon Column Observing Network's GGG2014 Data Version, Carbon Dioxide Information Analysis Center, Oak Ridge National Laboratory, Oak Ridge, Tennessee, USA, 10, doi:10.14291/tccon.ggg2014.documentation.R0/1221662, 2015.

York, D., Evensen, N. M., Martınez, M. L., and Delgado, J. D. B.: Unified equations for the slope, intercept, and standard errors of the best straight line, American Journal of Physics, 72, 367–375, 2004.